© 2017. Published by The Company of Biologists Ltd | Journal of Cell Science (2017) 130, 2405-2415 doi:10.1242/jcs.200477

RESEARCH ARTICLE

Arf6 and Rab22 mediate T cell conjugate formation by regulating clathrin-independent endosomal membrane trafficking

Debra L. Johnson[1,2], Jessica Wayt[1], Jean M. Wilson[2] and Julie G. Donaldson[1]

ABSTRACT

Endosomal trafficking can influence the composition of the plasma membrane and the ability of cells to polarize their membranes. Here, we examined whether trafficking through clathrin-independent endocytosis (CIE) affects the ability of T cells to form a cell–cell conjugate with antigen-presenting cells (APCs). We show that CIE occurs in both the Jurkat T cell line and primary human T cells. In Jurkat cells, the activities of two guanine nucleotide binding proteins, Arf6 and Rab22 (also known as Rab22a), influence CIE and conjugate formation. Expression of the constitutively active form of Arf6, Arf6Q67L, inhibits CIE and conjugate formation, and results in the accumulation of vacuoles containing lymphocyte function-associated antigen 1 (LFA-1) and CD4, molecules important for T cell interaction with the APC. Moreover, expression of the GTP-binding defective mutant of Rab22, Rab22S19N, inhibits CIE and conjugate formation, suggesting that Rab22 function is required for these activities. Furthermore, Jurkat cells expressing Rab22S19N were impaired in spreading onto coverslips coated with T cell receptor-activating antibodies. These observations support a role for CIE, Arf6 and Rab22 in conjugate formation between T cells and APCs.

KEY WORDS: Arf6, Rab22, Rab22a, Clathrin-independent endocytosis, T cell, Immunological synapse

INTRODUCTION

T cells are part of the adaptive immune system and use the T cell receptor (TCR) to recognize foreign peptides on the surface of antigen-presenting cells (APCs). Engagement of the TCR initiates T cell signaling, polarization and activation. This phenomena may last for several hours (Friedl and Storim, 2004; Griffiths et al., 2010), leading to cytokine production and increased proliferation (Zhu and Paul, 2008). The contact between the T cell and APC is a unique form of cell–cell contact and membrane trafficking is likely to be important for this interaction. In resting T cells, the TCR undergoes constitutive internalization via clathrin-mediated endocytosis (CME) (Crotzer et al., 2004). The TCR recycles back to the cell surface in a Rab11 (also known as Rab11a) (Liu et al., 2000) and sorting nexin 17 (SNX17)-dependent manner (Osborne et al., 2015). During activation, there is polarized recycling of the TCR, creating an accumulation at the synapse that allows for the proper signaling strength (Das et al., 2004; Griffiths et al., 2010). Other signaling proteins appear to enter cells by clathrin-independent endocytosis (CIE) (Balagopalan et al., 2009). However, little is known about the contribution of membrane movement through clathrin-independent forms of endocytosis and the effects that this trafficking has on T cell conjugate formation and activation.

Although there are many types of CIE, our laboratory has focused on a form that is associated with Arf6, a small guanine nucleotide-binding protein (G protein). We have defined this membrane trafficking system based on the cargo that traverses these endosomes and the Rab G proteins that control movement through the pathway (Maldonado-Baez et al., 2013b). The ubiquitously expressed major histocompatibility complex (MHC) class I (MHCI) (Radhakrishna and Donaldson, 1997) and peptide-loaded MHC class II (MHCII) (Walseng et al., 2008) both enter cells via CIE. MHCI enters cells in vesicles separate from those containing CME cargo, such as the transferrin receptor (TfR) proteins, but then meets with CME cargo proteins later, after fusing to sorting endosomes that are marked by Rab5 (Rab5a and Rab5b isoforms) and eventually by the early endosomal antigen 1 (EEA1). From there, MHCI is transported to late endosomes and lysosomes for degradation, or is trafficked to the endocytic recycling compartment (ERC) for recycling back to the cell surface (Naslavsky et al., 2003). We identified new cargo proteins [including CD44, CD98 (also known as SLC3A2) and CD147 (also known as basigin)] that take an itinerary that differs from MHCI in that they do not move to EEA1-associated compartments or lysosomes but return directly back to the cell surface (Eyster et al., 2009). For both types of cargo proteins, recycling back to the cell surface involves Rab11, Rab22 (also known as Rab22a) (Maldonado-Baez et al., 2013a; Weigert et al., 2004) and Arf6 (Radhakrishna and Donaldson, 1997). Furthermore, recycling of CIE cargo proteins back to the cell surface is critical for changes in cortical actin structure that occur during cell spreading (Song et al., 1998), cell migration (Powelka et al., 2004; Ratcliffe et al., 2016) and wound healing (Santy and Casanova, 2001).

The roles of Rab and Arf G proteins in T cells before and after activation have not been thoroughly investigated. Rab11 has been implicated in the targeting of lymphocyte-specific protein tyrosine kinase (Lck), to the immunological synapse (Griffiths et al., 2010) and for recycling of the TCR (Liu et al., 2000). Rab35 also plays a role in endosomal recycling of the TCR and is required for T cell activation (Patino-Lopez et al., 2008). One report has suggested that Arf6 inactivation is important for T cell conjugation (Tzachanis et al., 2003). On the other hand, Rab22, which is closely related to Rab5, has not been examined in T cells.

Here, we sought to characterize the function of clathrin-independent endosomal membrane trafficking in T cells. Using the Jurkat T cell line, we find these cells undergo dynamin-independent internalization of CIE cargo proteins at rates similar to other cells types. Arf6 mediates movement through this pathway and functional Rab22 is required for internalization. Furthermore, we find that Arf6 and Rab22 are essential for cell spreading and stable T cell conjugate formation.

[1]Cell Biology & Physiology Center, NHLBI, NIH, Bethesda, MD 20892, USA. [2]Department of Cellular & Molecular Medicine, University of Arizona, Tucson, AZ 85724, USA.

J.M.W., 0000-0001-9557-3458; J.G.D., 0000-0002-5241-5617

Received 6 December 2016; Accepted 30 May 2017

Journal of Cell Science

Journal of Cell Science (2017) 130, 2405-2415 doi:10.1242/jcs.200477

RESULTS

To study CIE in Jurkat T cells, we examined the internalization of two widely expressed canonical CIE cargo proteins, MHCI and CD98. MHCI is expressed on nearly all nucleated cells and, here, we use MHCI as a proxy for the CIE pathway. CD98 is the heavy chain of a neutral amino acid transporter (Deves and Boyd, 2000). Antibody internalization assays with monoclonal antibodies against MHCI (W6/32) and CD98 (MEM-108) were used to follow the trafficking of these cargo proteins, while fluorescently tagged transferrin was used to monitor CME. After 5 min of uptake at 37°C and removal of surface antibody, a few small puncta containing antibodies to MHCI were visible in the cell periphery that did not colocalize with transferrin, which was present in larger endocytic structures (Fig. 1A, top panels, arrowheads). After 30 min, MHCI

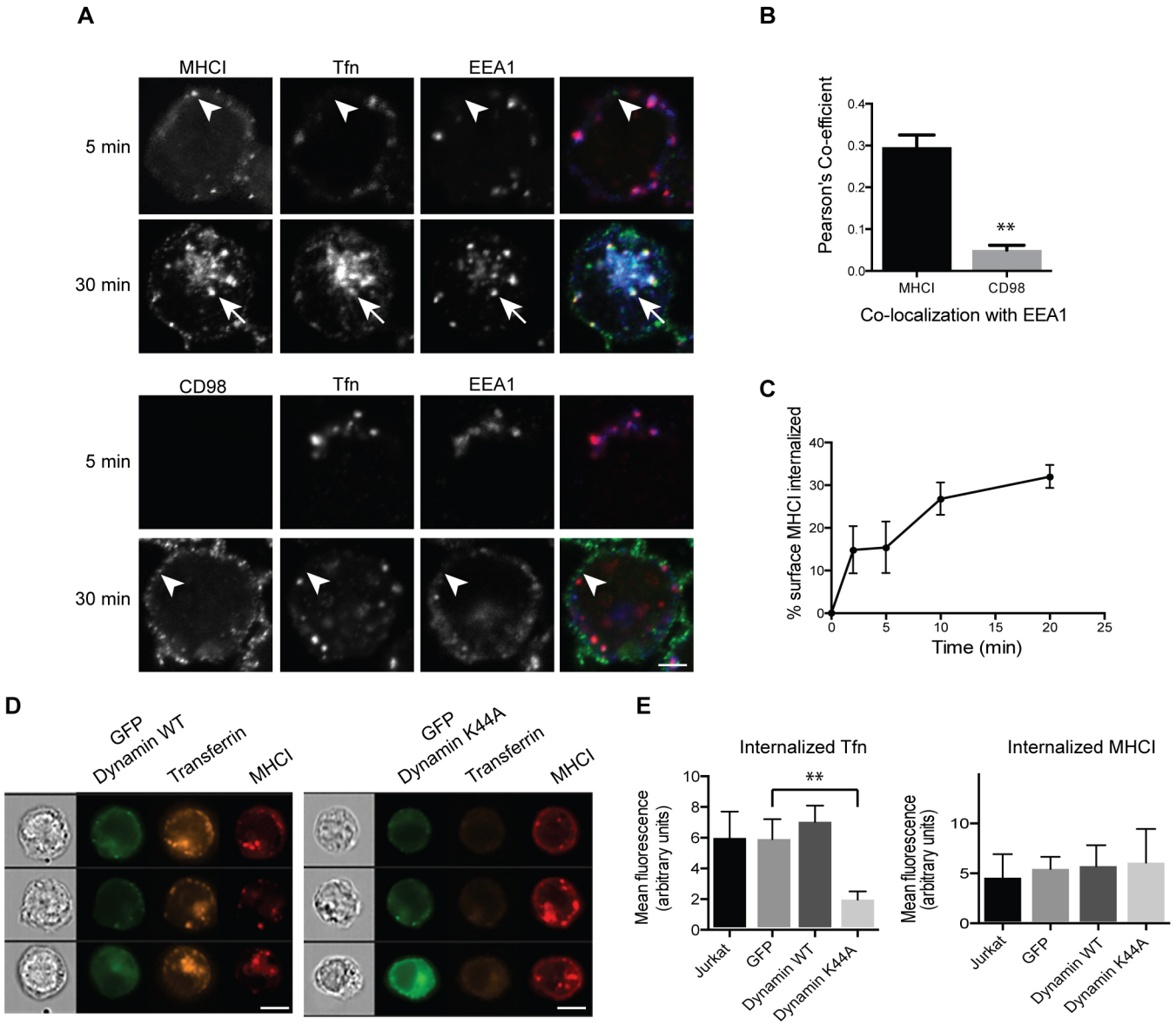

Fig. 1. Jurkat T cells internalize CIE cargo separately from transferrin, in a dynamin-independent manner, at a rate of 2% per minute. (A) Cells were incubated at 37°C with antibodies to MHCI or CD98 and Alexa Fluor 633-conjugated transferrin for 5 or 30 min. Bound surface antibodies were removed by treating cells with a low pH buffer for 8 s prior to fixation. Cells were immunolabeled with antibodies to EEA1, and fluorescent secondary antibodies were used to detect internalized MHCI and CD98 antibody. MHCI is in puncta that are distinct from transferrin-containing endosomes (arrowheads) at 5 min, indicating an entry mechanism distinct from CME. Note that at 30 min, MHCI and transferrin meet in a common endosome (arrows) and in the ERC. CD98 is in a distinct endosome (arrowhead) that does not colocalize with transferrin. Scale bar: 3 µm. (B) The Pearson's correlation coefficient shows a significant difference between the correlation of MHCI with EEA1, as compared to CD98 with EEA1, at the 30 min time point. Shown is the mean±s.e.m. of three experiments, with at least 42 cells measured in each experiment. $^{**}P<0.01$ (unpaired *t*-test). (C) Cells were incubated at 4°C with antibodies to MHCI. Cells were washed, returned to warm medium, fixed at indicated time points, and remaining surface antibody detected by fluorescent secondary antibodies and imaging flow cytometry. MHCI enters cells at a rate of ∼2% per minute. Shown is the mean±s.e.m. of four experiments. (D,E) Cells were transfected with GFP-tagged wild-type (WT) or K44A mutant dynamin, and then incubated at 37°C with antibodies to MHCI and Alexa Fluor 594-conjugated transferrin for 30 min. Bound surface antibodies were removed by treating cells with a low pH buffer for 8 s prior to fixation. (D) Sample images from imaging flow cytometry showing that there is a decrease in internalized transferrin in cells expressing dynamin K44A. Scale bars: 7 µm. (E) Quantification of internalized transferrin (Tfn) and MHCI by flow cytometry. Shown is the mean ±s.e.m. of four experiments (2000 cells scored/treatment). GFP–dynamin-K44A significantly reduces transferrin internalization but not MHCI internalization. $^{**}P<0.01$ (unpaired *t*-test).

Journal of Cell Science (2017) 130, 2405-2415 doi:10.1242/jcs.200477

was observed in endosomes that also contained transferrin and were positive for early endosomal antigen 1 (EEA1) (Fig. 1A, top panels, arrows). MHCI and transferrin-positive endosomes clustered in the juxtanuclear region, consistent with the location of the endocytic recycling compartment (ERC). Another CIE cargo protein, CD98, was not detected in intracellular compartments after 5 min of incubation. However, by 30 min, CD98-containing endosomes that did not colocalize with transferrin were observed in the periphery (Fig. 1A, bottom panels, arrowheads). Thus, in Jurkat cells, as in other cells, CIE cargo proteins are internalized separately from CME cargo proteins.

We have observed in several cell types that, after clathrin-independent internalization, CD98 is sorted away from MHCI, and MHCI moves into endosomes containing EEA1. CD98 avoids these EEA1-positive compartments due to an acidic cluster in the cytoplasmic tail (Eyster et al., 2009; Maldonado-Baez et al., 2013a). We checked to see whether Jurkat T cells also show evidence of such sorting by examining which cargo reached compartments marked by EEA1. After 30 min of internalization, MHCI endosomes colocalized with EEA1, whereas the small peripheral endosomes containing CD98 did not colabel with EEA1. This was quantified by determining the Pearson's correlation coefficient (Fig. 1B). CD98 colocalizes with EEA1 significantly less than MHCI, confirming that there is similar sorting of CIE cargo proteins in Jurkat T cells to what is observed in other cell types.

To determine the rate at which CIE occurs in Jurkat T cells, we performed flow cytometry endocytosis assays. We measured loss of surface-bound MHCI antibodies over time and found that surface MHCI was internalized at a rate of ~2% per minute (Fig. 1C). These rates for CIE are similar to those observed in other cell types (Naslavsky et al., 2003). Although CME is dependent upon dynamin for vesicle scission, most forms of CIE are independent of dynamin (Mayor et al., 2014). To determine whether dynamin is required for MHCI internalization, we expressed GFP-tagged wild-type dynamin or a dominant negative mutant of dynamin (K44A) and analyzed internalization by using imaging flow cytometry. Representative cell images (Fig. 1D) show that transferrin and MHCI entered cells expressing wild-type dynamin. Transferrin endocytosis, but not that of MHCI, was inhibited in cells expressing the K44A mutant of dynamin. Quantification of internalization showed that transferrin internalization in K44A-expressing cells was reduced to 30% the level found in control cells expressing wild-type dynamin; MHCI endocytosis was not affected (Fig. 1E). Thus, CIE in Jurkat T cells is similar to that in other human cell types; it occurs independently of dynamin, and CIE cargo are differentially trafficked after endocytosis.

Having shown that CIE occurs in Jurkat T cells, we wished to demonstrate that this endocytic process can also be observed in primary human T cells. Naive, CD4+ T cells were purified from human peripheral blood and incubated with antibodies to MHCI, CD98 and transferrin conjugated to Alexa Fluor 594 to assess endocytosis patterns. At 5 min MHCI could be observed in endosomes that did not contain transferrin (Fig. 2A, arrowheads) but after 30 min extensive colocalization between MHCI and transferrin was observed (Fig. 2A, arrows). After 30 min we also observed that MHCI colocalized with EEA1 whereas CD98 did not significantly colocalize with EEA1 (Fig. 2B). This difference in colocalization with EEA1 was quantified in Fig. 2C. From this, we conclude that primary human T cells also engage in CIE and that CIE cargo proteins (MHCI and CD98) are differentially handled, as was observed in Jurkat T cells and in other human cell lines.

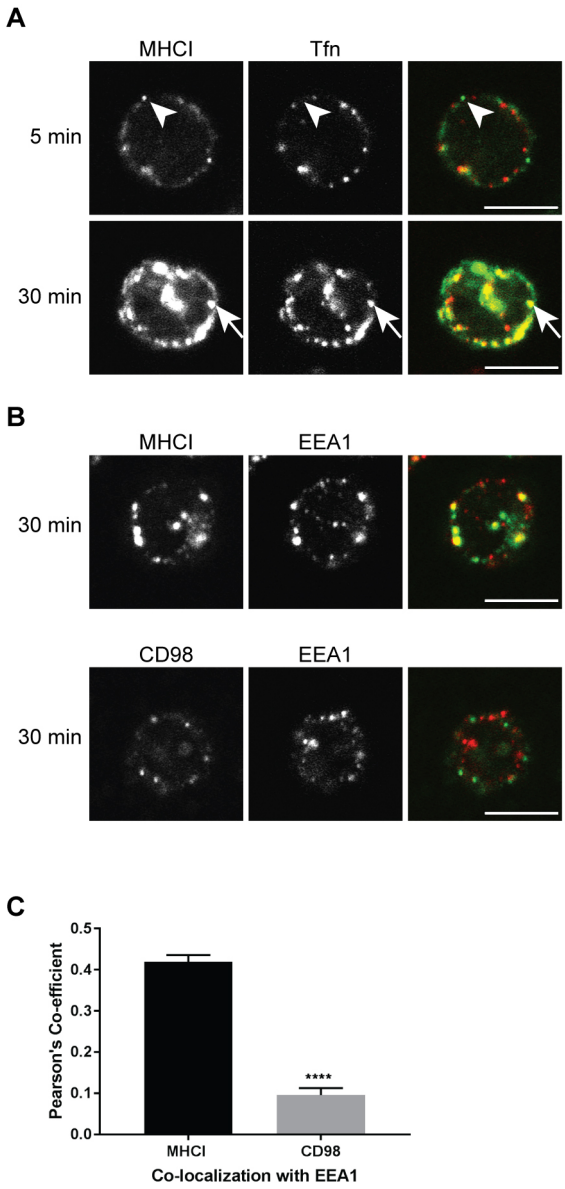

Fig. 2. CIE occurs in naive human T cells. (A) Naive, CD4+ human T cells were incubated with antibodies to MHCI and Alexa Fluor 594-conjugated transferrin for 5 or 30 min, and then treated with low pH buffer prior to fixation and labeling of internalized MHCI with Alexa Fluor 488-conjugated secondary antibody. Arrowhead highlights MHCI without transferrin; arrow highlights MHCI with transferrin. (B) T cells were incubated with antibodies to MHCI or CD98 for 30 min and then treated with low pH buffer prior to fixation and subsequent labeling for EEA1, and use of Alexa Fluor 488-conjugated secondary antibodies for detection of MHCI and CD98 and Alexa Fluor 594-conjugated secondary antibodies for EEA1. Scale bars: 5 µm. (C) The Pearson's correlation coefficient shows a significant difference between the correlation of MHCI with EEA1 as compared to CD98 with EEA1 at the 30 min time point. Shown is the mean±s.e.m. of three experiments, with at least 30 cells measured in each experiment. ****P<0.0001 (unpaired t-test).

Arf6 is associated with CIE cargo trafficking

In several cell types, Arf6 defines the CIE cargo pathway, as Arf6 is present at the cell surface and also on endosomes that contain CIE, but not CME, cargo proteins (Naslavsky et al., 2003, 2004; Radhakrishna and Donaldson, 1997). Therefore, we examined whether CIE cargo proteins colocalize with Arf6 and if their trafficking is influenced by Arf6 activity in Jurkat T cells. Jurkat T

Journal of Cell Science (2017) 130, 2405-2415 doi:10.1242/jcs.200477

cells were transiently transfected with plasmids encoding either wild-type Arf6 tagged with GFP (Arf6WT–GFP) or the constitutively active mutant of Arf6 tagged with GFP, Arf6Q67L–GFP. After 24 h, the cells were fixed and the steady-state distribution of cargo proteins was examined. MHCI colocalized with Arf6WT–GFP at the plasma membrane as well as on some internal structures (Fig. 3A, arrows). Expression of Arf6Q67L–GFP induces the accumulation of enlarged endocytic structures that contain CIE cargo proteins (Brown et al., 2001; Naslavsky et al., 2003, 2004). These structures were also formed in Jurkat T cells upon expression of Arf6Q67L–GFP, and they were positive for MHCI (Fig. 3A, arrows).

The trafficking of T cell plasma membrane proteins is relatively uncharacterized. We examined whether other proteins colocalized at steady-state with Arf6. Integrins have been shown to traffic via CIE and accumulate in Arf6Q67L-containing vacuoles (Brown et al.,

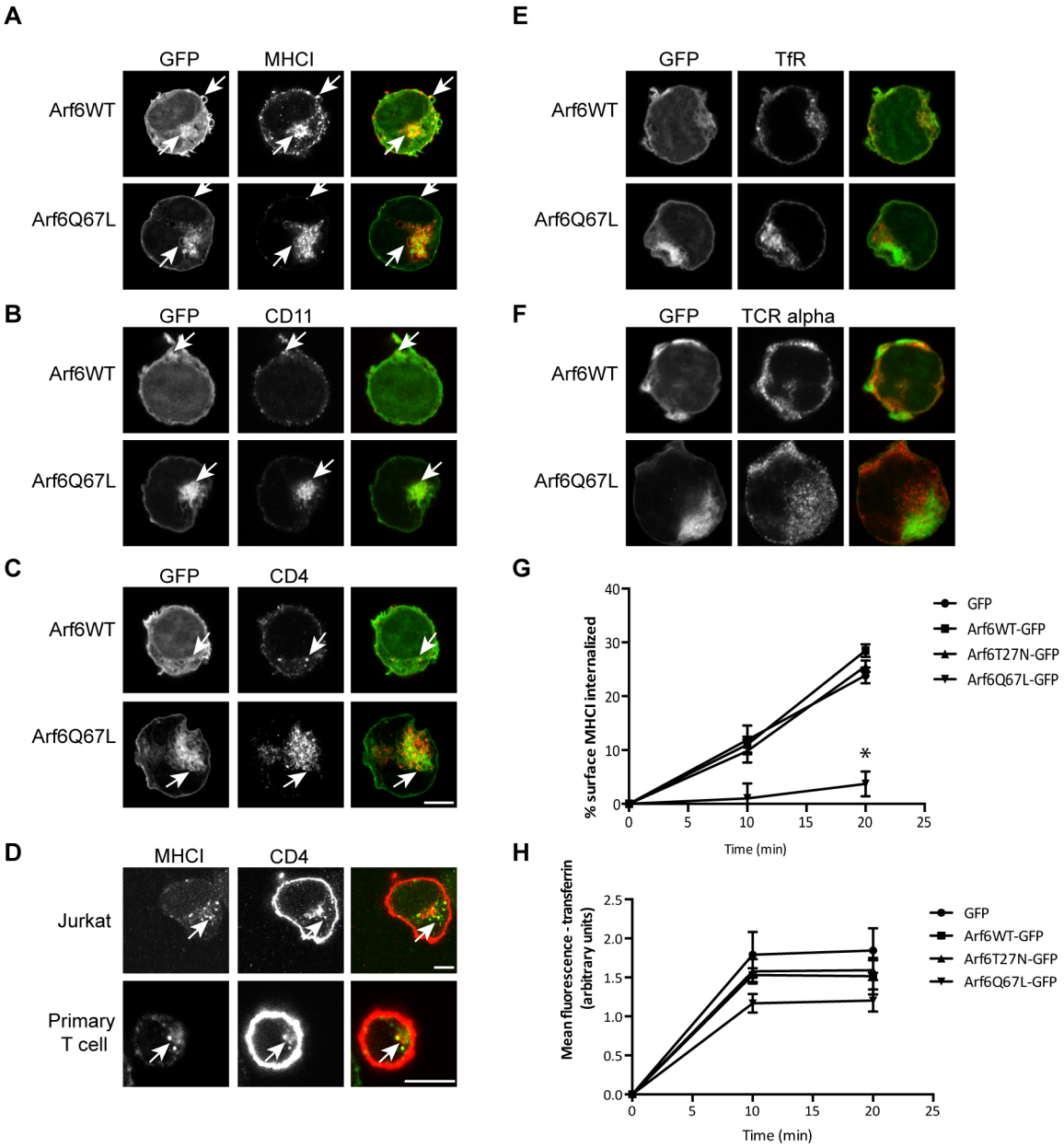

Fig. 3. Arf6 colocalizes with CIE cargo proteins that are important for T cell activation and Arf6Q67L inhibits CIE in Jurkat T cells. Cells were transiently transfected with Arf6WT–GFP or Arf6Q67L–GFP. After fixation, the steady state distribution of cargo proteins was assessed with antibodies, followed by labeling with Alexa Fluor 594-conjugated secondary antibodies. MHCI (A), CD11 (LFA-1) (B), and CD4 (C) colocalize with Arf6WT and Arf6Q67L. CME cargo proteins transferrin receptor (E) and T cell receptor α (F) do not colocalize with Arf6-positive membranes. Scale bars: 3 µm. (D) Jurkat T cells and primary T cells were incubated with antibodies to MHCI for 30 min, treated with a low pH wash, then fixed and stained with antibodies to CD4, followed by use of Alexa Fluor 488-secondary antibody to detect MHCI and Alexa Fluor 594-secondary antibodies to detect CD4. Scale bars: 5 µm. Arrows highlight cargo-containing endosomes. (G,H) Cells were chilled to 4°C and incubated with antibodies to MHCI (G) or fluorescently conjugated transferrin (H). Cells were rinsed and warmed for the indicated times to allow internalization of antibody-bound MHCI and transferrin. Remaining surface MHCI and internalized transferrin were measured by using imaging flow cytometry. Expression of Arf6Q67L inhibits internalization of the CIE cargo protein MHCI but not the CME cargo protein transferrin receptor, as measured by determining transferrin internalization. Shown are the mean±s.e.m. for four experiments. For the 20 min time point, cells expressing Arf6Q67L internalized less MHCI than GFP controls. *P<0.05 (unpaired t-test).

Journal of Cell Science (2017) 130, 2405-2415 doi:10.1242/jcs.200477

2001). We examined whether LFA-1, an integrin important for T cell interactions, was present on these vacuoles. As shown in Fig. 3B (arrows), labeling of CD11, the integrin α-L subunit of lymphocyte function-associated antigen 1 (LFA-1), colocalized with Arf6Q67L–GFP-containing vacuoles, suggesting that LFA-1 travels in CIE membrane trafficking pathways. Furthermore, CD4, a co-receptor of the TCR, does not possess a strong CME targeting signal in its un-phosphorylated form and is believed to enter cells by CIE until it becomes phosphorylated (Pelchen-Matthews et al., 1993; Pitcher et al., 1999). Like MHCI, CD4 was sequestered in the Arf6Q67L–GFP-induced vacuoles (Fig. 3C arrows), suggesting that CD4 is a CIE cargo protein in resting T cells. The steady state distribution of CD11 and CD4 in Arf6Q67L-induced vacuoles is consistent with these cargo proteins entering the cells by CIE. In contrast, known CME cargo proteins, including TfR proteins (Fig. 3E) and TCRα (encoded by *TRA*), a subunit of the T cell receptor (Fig. 3F), did not localize with either Arf6WT–GFP or Arf6Q67L–GFP. We made attempts to look at internalization of CD4 and CD11 using antibody internalization assays. For CD4, we could not find an antibody suitable for this assay; however, to support the contention that CD4 is present on MHCI-containing endosomes, we allowed Jurkat and primary human T cells to internalize antibodies to MHCI and then labeled the fixed cells with antibodies to CD4. CD4 was on the surface of both cells but also colocalized with MHCI at endosomal compartments (Fig. 3D, arrows). For CD11, we examined the effects of expression of the wild-type and K44A mutant of dynamin on endocytosis and found that CD11 endocytosis was not affected by dynamin K44A expression while transferrin endocytosis was blocked (Fig. S1).

In HeLa cells, Arf6 is not required for CIE but it is required for recycling of CIE cargo proteins, as expression of Arf6T27N inhibits recycling (Naslavsky et al., 2003, 2004; Powelka et al., 2004; Radhakrishna and Donaldson, 1997). In contrast, expression of Arf6Q67L, with time, results in a halt in CIE as the vacuoles accumulate and trap membrane (Brown et al., 2001). We examined the effects of expression of Arf6WT–GFP, Arf6T27N–GFP and Arf6Q67L–GFP on endocytosis of MHCI and transferrin with a flow cytometry assay. We found that MHCI internalization was not affected by expression of Arf6T27N–GFP but was severely inhibited in cells expressing Arf6Q67L–GFP (Fig. 3G). Internalization of transferrin receptor was not affected by expression of any Arf6 mutant in the Jurkat cells (Fig. 3H).

Rab22 partially colocalizes with MHCI and is required for CIE

Rab22 is associated with recycling of endosomal cargo in many cell types (Magadan et al., 2006; Maldonado-Baez and Donaldson, 2013; Weigert et al., 2004) but its role in T cells is unknown. We examined whether Rab22 is associated with CIE membranes in Jurkat T cells and whether its activity alters the trafficking of CIE cargo. We expressed GFP-tagged wild-type Rab22, and its inactive (S19N) and active (Q64L) mutants, in Jurkat T cells and assessed MHCI internalization. In cells expressing Rab22Q64L, MHCI was observed in enlarged endosomes that colocalized with Rab22 (Fig. 4A, middle panels). However, in cells expressing Rab22S19N there was very little internal MHCI, and Rab22 was mostly cytosolic in distribution. In contrast, internalized transferrin was unaffected in cells expressing any of the Rab22 forms (Fig. 4A). We quantified the internalization of MHCI and transferrin in cells expressing Rab22, Rab22S19N or Rab22Q64L by imaging flow cytometry. In agreement with confocal imaging, MHCI internalization was greatly diminished in cells expressing the dominant-negative form of Rab22, Rab22S19N, when compared to that observed in untransfected or Rab22 wild-type-transfected cells (Fig. 4B), suggesting that Rab22 is required for internalization of MHCI in Jurkat T cells. Interestingly, in cells expressing Rab22Q64L there was a delay in endocytosis of MHCI at 10 min but the amount of MHCI internalized equaled that of untransfected cells by 20 min. This delay might be due to entry of MHCI into the larger macropinosome-type structures that are observed in confocal imaging (Fig. 4A, middle panel). Transferrin internalization was not affected by expression of Rab22 or any of its mutants (Fig. 3B).

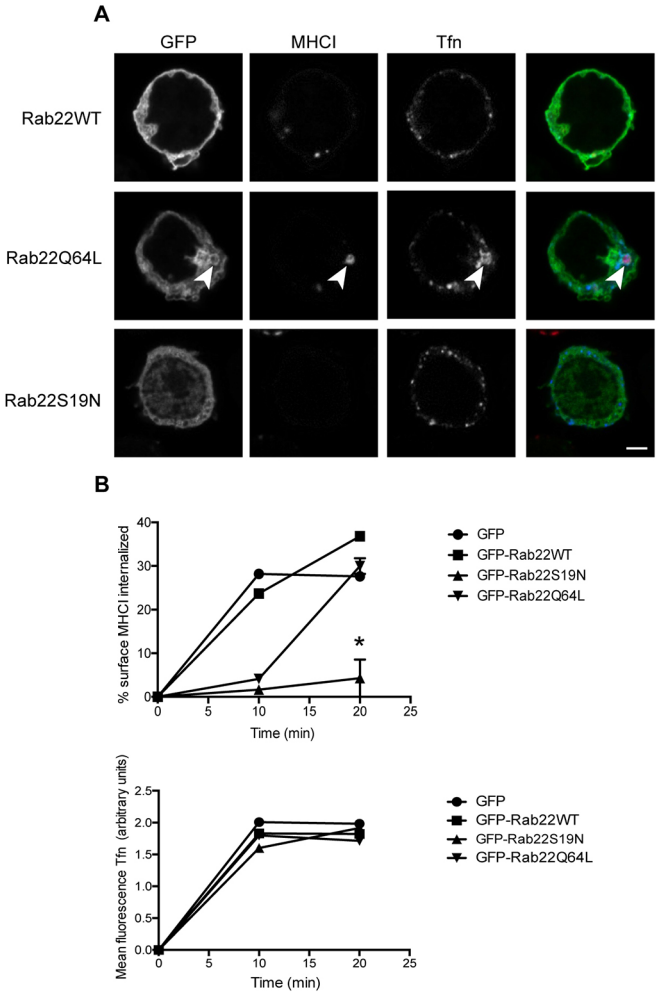

Fig. 4. Rab22 is required for internalization of MHCI. Cells were transiently transfected with GFP-tagged Rab22WT, Rab22Q64L or Rab22S19N and incubated at 37°C with antibodies against MHCI and Alexa Fluor 647-conjugated transferrin to allow endocytosis. Surface antibody was removed by a low pH rinse and then cells were fixed after 30 min and primary antibody was detected with Alexa Fluor 594 secondary antibodies. (A) Confocal imaging shows that expression of Rab22Q64L results in the formation of large endosomes that are positive for MHCI (arrowheads). MHCI is not internalized in cells expressing Rab22S19N. Scale bar: 3 µm. (B) Imaging flow cytometry was used to quantify uptake of CIE and CME cargo. Rab22S19N inhibits internalization of MHCI but not of transferrin. Shown are the mean±s.e.m. for three experiments. For the 20 min time point, cells expressing Rab22S19N internalized less MHCI than GFP controls. *P<0.05 (unpaired t-test).

Taken together, these observations demonstrate that dynamin-independent CIE exists in Jurkat T cells, and that CIE trafficking is regulated by Arf6. However, we find that Rab22 is required for endocytosis of MHCI in Jurkat cells, a finding that contrasts with the role of Rab22 in recycling of MHCI in other cell types (Maldonado-Baez and Donaldson, 2013; Weigert et al., 2004).

Journal of Cell Science (2017) 130, 2405-2415 doi:10.1242/jcs.200477

The Arf6 GTPase cycle is required for T cell conjugate formation

In mammalian cells, CIE and the trafficking of CIE endosomal membranes are critical for changes in the cortical actin cytoskeleton. Arf6 is required for the recycling of integrin back to the cell surface (Powelka et al., 2004; Ratcliffe et al., 2016) and more generally has been implicated in cell spreading (Song et al., 1998) and cell migration (Santy and Casanova, 2001). The observation that CD4 and LFA-1, important molecules involved in T cell activation and synapse formation, localized to the vacuoles formed in cells expressing Arf6Q67L suggests that CIE endosomal membrane trafficking might impact T cell activity.

To test the role of Arf6 in immune synapse formation, we examined the ability of Jurkat T cells to form synapses with an APC by using Raji cells, a B cell lymphoma line that can be treated with Staphlococcal enterotoxin E (SEE) and serve as an APC. First, we examined the localization of Arf6WT–GFP and the presence of phosphorylated tyrosine, a general marker for T cell activation, during synapse formation in activated and non-activated samples. In non-activated samples, Arf6WT–GFP and its mutants did not polarize to the site of contact with an APC (Fig. 5A). The level of phosphorylated tyrosine was generally low in these samples, although Arf6Q67L-expressing cells appeared to have slightly more phosphorylated tyrosine at the plasma membrane. However, in activated samples, Arf6WT–GFP polarized to the site of contact with the APC while Arf6T27N–GFP remained throughout the cell (Fig. 5B). In cells expressing Arf6Q67L, the cells did not form an immunological synapse near the Arf6Q67L-associated vacuoles. This may be due to the fact that these vacuoles do not contain enough dynamic membrane required for conjugate formation (see below). Arf6WT–GFP also colocalized with phosphorylated tyrosine at the site of contact with the APC. In cells expressing the dominant-negative Arf6T27N, there was an altered pattern of phosphorylated tyrosine at the contact site, consisting of small punctate structures at the plasma membrane (Fig. 5B, middle panel).

We quantified the efficiency of conjugate formation in cells expressing Arf6 mutants by imaging flow cytometry. Cells expressing either Arf6T27N or Arf6Q67L showed diminished capacity to form stable conjugates (Fig. 5C). Another way to examine this defect is to monitor the ability of the cells to spread on anti-CD3-coated activating coverslips. Indeed, we found that cells expressing Arf6Q67L or Arf6T27N were inhibited in spreading on activated coverslips (Fig. 5D). Even expression of wild-type Arf6 impaired spreading when compared to GFP alone (Fig. 5D), consistent with overexpression of wild-type Arf6 in cells leading to more of an activated phenotype. Although cells expressing Arf6Q67L or Arf6T27N were impaired in spreading on the activated coverslip, the amount of phosphorylated ZAP70 present, used as an indication of T cell activation, was not significantly altered (data not shown). Taken together, these findings suggest that both internalization and recycling of CIE cargo proteins, influenced by Arf6 activities, are required for efficient conjugation.

Rab22 is required for T cell conjugate formation and cell spreading

Next, we examined the effect of expression of Rab22 active and inactive mutants on T cell conjugate formation. In samples without SEE (non-activated) neither Rab22WT nor its mutants polarized in places of contact with the APC and phosphorylated tyrosine levels were low (Fig. 6A). In samples treated with SEE (activated), overexpressed Rab22WT and Rab22Q64L polarized to the site of contact with an APC (Fig. 6B). However, there were few cells expressing Rab22S19N that formed conjugates. We quantified the efficiency of conjugate formation and found that cells expressing Rab22S19N have decreased efficiency of conjugation (Fig. 6C). By contrast, cells expressing wild-type or Rab22Q64L have similar levels of conjugate formation to that seen in GFP-expressing cells (Fig. 6C). It was striking that expression of Rab22S19N impaired both CIE and the ability of T cells to form stable conjugates. We also assessed the effect of expression of Rab22 mutants on Jurkat T cell spreading on anti-CD3-coated activating coverslips. Cells expressing either the wild-type Rab22 or Rab22Q64L spread as effectively as GFP-expressing cells on these coverslips (Fig. 6D). However, cells expressing Rab22S19N were deficient in spreading on the coverslips (Fig. 6D). These findings demonstrate that Rab22 is necessary for Jurkat cell conjugate formation and spreading on activating coverslips.

DISCUSSION

As part of the adaptive immune response, $CD4^+$ T cells become activated after contact with APCs displaying foreign peptides on MHC class II molecules. In the animal, this interaction can last for hours as the APC moves around the lymph node (Miller et al., 2004). Such an interaction must be specific and of high avidity, and thus an elaborate immunological synapse can be formed. A role for endosomal trafficking has been suggested for synapse formation (Balagopalan et al., 2009; Griffiths et al., 2010). Whether CIE and subsequent membrane movement through the CIE pathway are also involved in T cell–APC conjugate formation has not been previously examined.

We find that CIE exists in Jurkat T cells and that it is similar to what was previously observed in HeLa cells (Eyster et al., 2009). Two prototypical CIE cargo proteins, MHCI and CD98, enter cells in a clathrin-independent manner. After internalization, MHCI moves to EEA1-containing compartments, whereas CD98 remains in the periphery and does not reach these later compartments. CIE cargo proteins colocalize with Arf6 and expression of Arf6Q67L led to formation of enlarged vacuolar structures that contained CIE cargo proteins including CD4 and LFA1. As a consequence of this accumulation, CIE is compromised and the efficiency of conjugate formation is impaired. Furthermore, expression of inactive Rab22 causes a marked inhibition of CIE and conjugate formation. Cells expressing inactive Rab22 are also defective at spreading on activating surfaces. Taken together, these findings provide compelling evidence that CIE and the trafficking of CIE cargo proteins are important for the initial connection between T cells and their APCs.

Although we found evidence of a role for CIE pathways in the efficiency of Jurkat cell conjugate formation, once conjugates were formed, there was no evidence of a defect in T cell activation. This suggests that the impairment we observe is upstream of T cell signaling. Interestingly, a recent paper reports on initial T cell–APC interaction that involves microvillar contacts that are independent of downstream T cell signaling (Cai et al., 2017).

A feature of CIE membrane trafficking systems is that their cycling into and out of the cell is important for changes in cell surface morphology necessary for cell spreading, migration, wound healing and metastasis (Grant and Donaldson, 2009). This is accomplished in part by the action of Arf6 on PI4P5 kinase and facilitation of actin rearrangements (Brown et al., 2001; Radhakrishna et al., 1996; Song et al., 1998), and the recycling of integrins (Powelka et al., 2004) and syndecans (Zimmermann et al., 2005) back to the cell surface through this pathway. The trapping of CD4 and LFA1 in Arf6Q67L-containing vacuoles may be

Journal of Cell Science (2017) 130, 2405-2415 doi:10.1242/jcs.200477

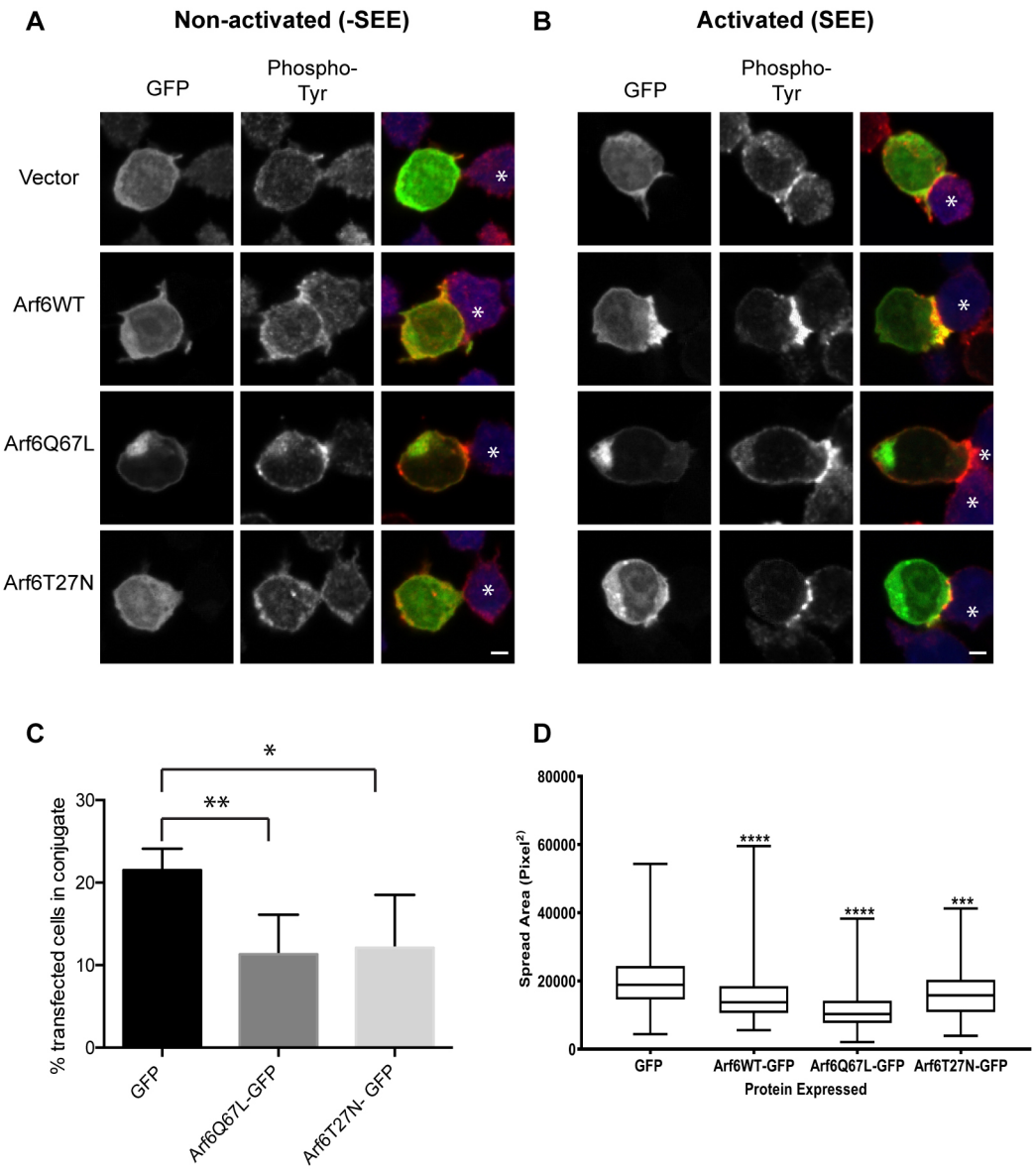

Fig. 5. Arf6 polarizes to the immunological synapse, and expression of Arf6T27N or Arf6Q67L reduces formation of stable T cell/APC conjugates. Jurkat T cells were transfected with GFP-tagged Arf6WT, Arf6Q67L or Arf6T27N. Jurkat cells were then incubated with APCs or with APCs that had been exposed to SEE. Cells were fixed, and phosphorylated tyrosine was detected with antibodies. (A) The non-activated control (-SEE) shows no polarization of Arf6 at the site of contact with the APC and there is only a small amount of phosphorylated tyrosine in the Arf6WT- and Arf6T27N-expressing cells. (B) In the activated sample (+SEE), Arf6WT and Arf6Q67L polarize towards the site of contact and colocalize with phosphorylated tyrosine. Arf6T27N does not polarize toward the site of contact and alters the phosphorylated tyrosine pattern. Scale bar: 3 µm. Asterisks mark APCs. (C) Cells expressing GFP alone, Arf6T27N or Arf6Q67L were incubated with APCs that had been exposed to SEE. After 1.5 h, cells were fixed and conjugate formation was quantified by using imaging flow cytometry. Shown are the mean±s.d. for four experiments. *P<0.05, **P<0.01 (unpaired t-test). (D) Jurkat cells expressing GFP-tagged Arf6WT, Arf6Q67L or Arf6T27N, or GFP alone, were plated on coverslips coated with antibodies against the T cell receptor (anti-CD3 antibody) for 3 min and then fixed and stained with a plasma membrane cell mask. The area of cell spread was quantified by using the image analysis software package Metamorph. Data is presented as box-and-whisker plots representing the median and the 25th and 75th percentiles. Whiskers show the minimum to maximum. n>150 cells over three independent experiments. ****P<0.0001 (one-way Anova with Kruskal–Wallis test).

responsible for the defect in conjugate formation that we observe in this study. Although we provide some evidence that CD4 and LFA-1 might be CIE cargo proteins in resting cells, we have not examined this in detail. Further work on these specific proteins will shed light on their endocytic trafficking. The recycling of both TCR and LFA-1 has been shown to be dependent upon the sorting nexin SNX17 (Osborne et al., 2015).

Arf6 was previously described as being upregulated in anergic (immunologically tolerant) T cells, and expression of Arf6Q67L has been shown to perturb the actin rearrangements that occurred upon T cell activation (Tzachanis et al., 2003). In agreement with that study, expression of Arf6Q67L results in the formation of vacuoles and altered actin cytoskeleton (Brown et al., 2001). When T cells expressing Arf6Q67L were incubated with the APCs, the vacuoles are positioned at the rear of the cell (Fig. 5B). A recent study described an early event in T cell activation where the initial adhesion triggers what they refer to as the anti-synapse, a transient signaling hub containing many signaling molecules distal to the

Journal of Cell Science (2017) 130, 2405-2415 doi:10.1242/jcs.200477

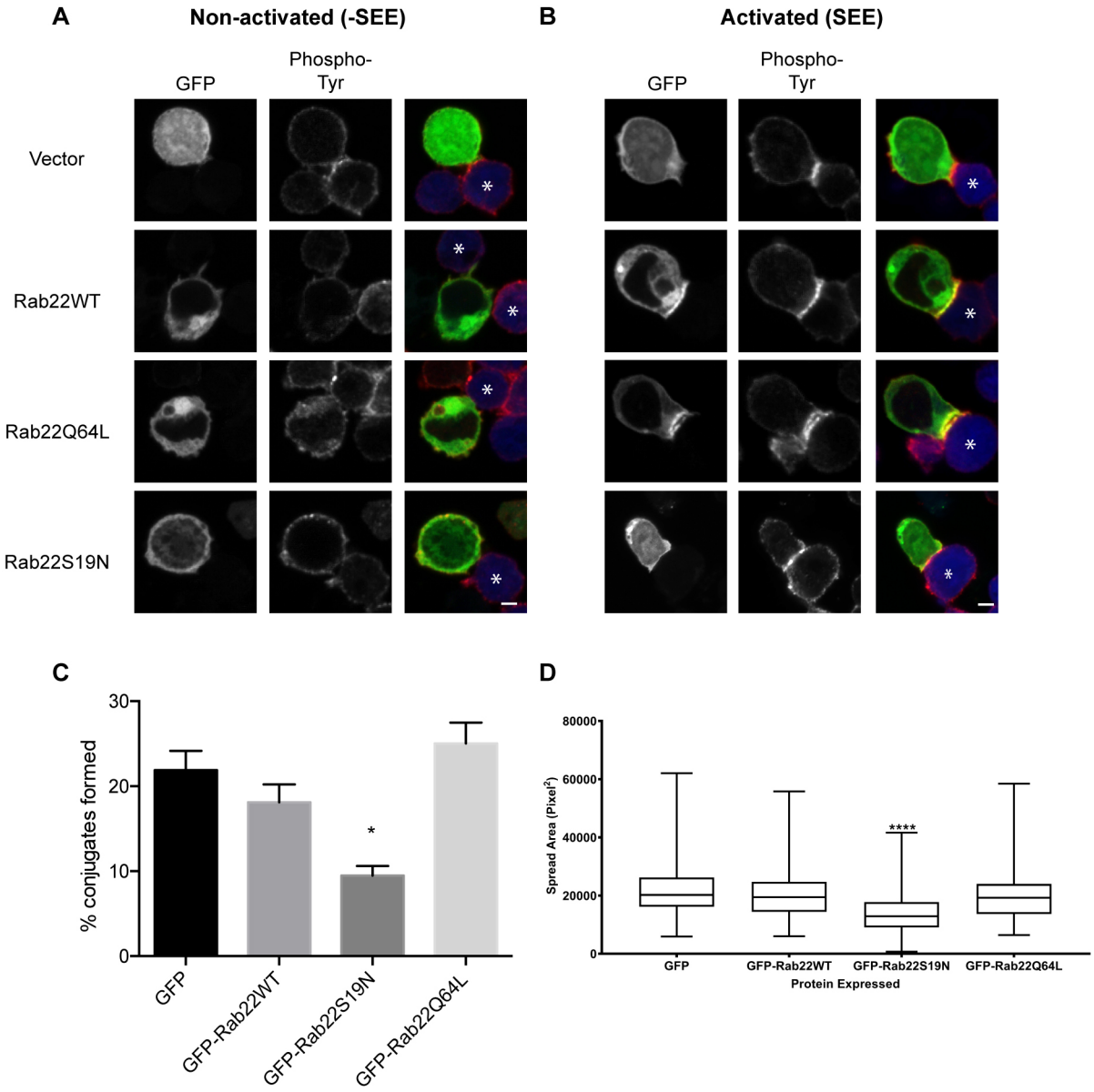

Fig. 6. Rab22 polarizes to the immunological synapse and is required for the formation of stable T cell–APC conjugates. Jurkat cells were transfected with GFP-tagged Rab22WT, Rab22Q64L or Rab22S19N. Jurkat cells were then incubated with APCs or with APCs that had been exposed to SEE. Cells were fixed and phosphorylated tyrosine was detected with antibodies. (A) The non-activated control (-SEE) shows no polarization of Rab22 at the site of contact with the APC and phosphorylated tyrosine is low. (B) In the activated sample (+SEE), Rab22WT and Rab22Q64L polarize toward the site of contact and colocalize with phosphorylated tyrosine on the plasma membrane. Rab22S19N does not polarize toward the site of contact and reduces phosphorylated tyrosine at the site of contact. Asterisks mark APCs. Scale bars: 3 µm. (C) Cells expressing GFP or GFP-tagged Rab22 were incubated with APCs that had been exposed to SEE. After 1 h, cells were fixed and conjugate formation was quantified by using imaging flow cytometry. Shown are mean±s.d. from three experiments. *P<0.05 (unpaired t-test). (D) Jurkat cells expressing GFP-tagged Rab22WT, Rab22Q64L or Rab22S19N, or GFP alone, were plated on coverslips coated with antibodies against the T cell receptor (anti-CD3 antibody) for 3 min and then fixed and stained with a plasma membrane cell mask. The area the cell spread was quantified by using the image analysis software package Metamorph. Data is presented as box-and-whisker plots representing the median and the 25th and 75th percentiles. Whiskers show the minimum and maximum. n>150 cells over at least three independent experiments. ****P<0.0001 (one-way Anova with Kruskal–Wallis test).

immune synapse (Guedj et al., 2016). The sequestered Arf6Q67L vacuoles are located at this site and thus are reminiscent of this anti-synapse. Another recent study identified a Rab11–FIP3–Rac1 signaling hub as being important for orchestrating actin remodeling during T cell activation (Bouchet et al., 2016). Since Arf6 also binds to FIP3 (also known as IKBKG), the influence of Arf activity on T cell conjugate formation observed here could be related to this finding. Interestingly, cytohesin 1, a guanine nucleotide exchange factor for Arf1 and Arf6, was originally identified as a protein that enhanced adhesion of LFA-1 to ICAM-1 on the APC (Kolanus et al., 1996). Although we did not look directly at cytohesin 1 here, we previously showed it is recruited by Arf6-GTP to the plasma membrane (Cohen et al., 2007) where it can enhance the activities of Arf6 (Santy and Casanova, 2001) and Arf1 (Cohen et al., 2007).

Related to the findings with active forms of Arf6, an earlier study reported blocks to immunological synapse formation upon expression of either dominant-negative forms of Rab35 or expression of EPI64C (also known as TBC1D10C), a Rab35

Journal of Cell Science (2017) 130, 2405-2415 doi:10.1242/jcs.200477

GTPase-activating protein (GAP) (Patino-Lopez et al., 2008). The phenotype observed, formation of enlarged vacuolar structures, is similar to the phenotype seen upon expression of Arf6Q67L observed here. This may be due to the finding that Arf6 and Rab35 are mutual antagonists that recruit each other's GAPs (Chaineau et al., 2013). Since Rab35 is delivered through CME and Arf6 is associated with CIE, these two G proteins coordinate input from the two entry pathways (Dutta and Donaldson, 2015).

Rab22 is closely related to Rab5, the key Rab protein associated with the sorting endosome, where initial sorting of incoming cargo proteins occurs. It was originally described as a Rab that also could recruit EEA1 (Kauppi et al., 2002) and more recently has been shown to recruit Rabex5, a GEF for Rab5 (Zhu et al., 2009). However, some studies place Rab22 at the level of recycling of CME (Magadan et al., 2006) and CIE (Barral et al., 2008; Weigert et al., 2004) cargo proteins. Unexpectedly, we find that Rab22 was required for CIE in Jurkat T cells and is also required for conjugate formation, suggesting that CIE is required for conjugate formation. It is important to note that since expression of Rab22S19N blocked CIE in Jurkat T cells, we could not assess whether it also impaired endosomal recycling. Interestingly, a recent study in dendritic cells has shown that Rab22 is required for recycling of MHCI and is important for cross presentation (Cebrian et al., 2016). There have been other reports of Rab22 acting at endocytic entry points. It is notable that Rab22 is required for endocytosis of the TrkA receptor and neurite outgrowth (Wang et al., 2011) and also that Rab22 functions first in the early uptake of the bacterium *Borrelia*, followed by activation of Rab5 (Naj and Linder, 2015). Yet another novel function for Rab22 may be an involvement in release of microvesicles from cells in response to hypoxia (Wang et al., 2014). Rab22, being a specialized and vertebrate-specific Rab protein, might play an important role in immune synapse formation in the animal.

Here, we provide evidence that the flow of membrane through endosomal compartments loaded by CIE is important for the proper function of T cells. CIE is also likely important for other cells of the immune system. For example, peptide-loaded MHC class II molecules are also continually endocytosed through CIE (Walseng et al., 2008). Furthermore, it has recently been appreciated that the trafficking of MHCI through CIE pathways could lead to opportunities for cross presentation (Blander, 2016). Further work will define the pathways and effectors that regulate these pathways.

MATERIALS AND METHODS

Cells, reagents and antibodies

Jurkat T cells (clone E7.6) were obtained from Dr Lawrence Samelson (National Cancer Institute, Bethesda, MD). Raji cells were purchased from ATCC (clone CCL-86). Jurkat and Raji cells were maintained at 37°C in 5% CO_2. They were cultured in Iscove's modified Dulbecco's GlutaMAX (IMDM) medium (ThermoFisher Scientific) supplemented with 10% fetal bovine serum (FBS; Lonza) and non-essential amino acids (ThermoFisher Scientific). Human T cells were isolated from a peripheral blood lymphocyte sample (provided by the Nihal Altan-Bonnet laboratory, NHLBI) using the Naive CD4+ cell isolation kit II (Miltenyi Biotec Inc.).

Poly-L-lysine solution was purchased from Sigma-Aldrich and used at 0.1% (w/v). Staphylococcal enterotoxin E was acquired from Toxin Technologies (Sarasota, FL). Transferrin conjugated to Alexa Fluor 594, 633 or 647, Cell Tracker Blue CMAC Dye and Cell Mask™ Deep Red plasma membrane stain were all products of ThermoFisher Scientific and were used in accordance with the manufacturer's instructions.

Antibodies used for endocytosis assays were mouse anti-MHCI (clone W6/32, 1:500; Biolegend), mouse anti-CD98 (clone MEM-108, 1:1000; Biolegend) and mouse anti-CD11 (clone G43-25B, 1:30; BD Biosciences). Antibodies for immunofluorescence and immunoblotting were as follows: rabbit anti-EEA1 (1:400, Cell Signaling), mouse anti-LFA-1 (CD11a) (clone HI111, 1:500; Biolegend), mouse anti-CD4 (clone Q4120, 1:400; Abcam), mouse anti-T cell receptor α (clone H-142, 1:200; Santa Cruz Biotechnology), mouse anti-transferrin receptor (clone DF1513, 1:500, Sigma-Aldrich), rabbit anti-phosphorylated tyrosine (Cat. #8954, 1:500, Cell Signaling). Secondary antibodies include donkey anti-mouse-IgG conjugated to Alexa Fluor 488, goat anti-rabbit-IgG conjugated to Alexa Fluor 594, and goat anti-mouse-IgG conjugated to Alexa Fluor 594 (ThermoFisher Scientific), all used at 1:1000.

DNA constructs and transient transfection

Human GFP-tagged Rab22 (accession NM_020673), Rab22S19N and Rab22Q64L were in pEGFP vector as described previously (Maldonado-Baez et al., 2013a). The human Arf6 (accession no. NM_001663) plasmid construction was described previously (Honda et al., 2005). Dynamin constructs were obtained from Mark McNiven (Mayo Clinic, Rochester, MN).

Jurkat cells were transfected using Amaxa Nucleofector Kit V (Lonza). For each transfection, 1.8×10^6 cells were pelleted in a 15 ml conical tube. Medium was aspirated, and cells were re-suspended in 100 µl room temperature Nucleofector Solution V. Plasmid DNA (3 µg) was added to each transfection. Cells were electroporated using Amaxa Program X-005 for high efficiency. Cells were incubated at room temperature for 10 min and then transferred to 2 ml warm, pre-equilibrated IMDM in a six-well plate. Cells were incubated for at least 15 h before further processing.

Immunofluorescence

Glass coverslips (#1.5, Fisher Scientific) were soaked in nitric acid for 45 min. Coverslips were then extensively washed in distilled water (dH_2O) and soaked overnight in clean water. Coverslips were dried and coated with 0.1% poly-L-lysine solution for at least 1 h and no longer than 24 h. Coverslips were then rinsed in PBS and dried completely before plating cells at a concentration of $\sim3\times10^5$ cells in 200 µl of complete medium. Cells were incubated at 37°C for 10 min to allow for adherence and then fixed in 4% formaldehyde for 15 min and rinsed in PBS, and non-specific blocking was reduced by using PBS with 1% FBS throughout antibody labeling. Cells were permeablized with 0.02% saponin and incubated with primary antibody for at least 2 h. Coverslips were rinsed and incubated with secondary antibodies for at least 1 h. Coverslips were mounted with ProLong Gold (ThermoFisher Scientific) and imaged with the Zeiss LSM780 or the Zeiss LSM880 microscope with a 63×1.4 NA Plan-Apochromat oil immersion objective lens. Colocalization was measured by using Zeiss Zen Blue Software.

Imaging flow cytometry

Samples for flow cytometry were processed in a 5 ml snap cap tubes. Cells were fixed in 4% formaldehyde for 15 min with rocking, and non-specific blocking was reduced with 1% FBS in PBS. Cells were permeabilized with 0.02% saponin, incubated with primary antibody for at least 2 h and incubated with secondary antibody for at least 1 h. All incubations were performed with rocking. Imaging flow cytometry was conducted on the ImageStreamX Mark II (EMD Millipore). Data was collected with a 60× objective with a minimum of 2000 cells collected for each sample, and compensation was performed for each color channel used. Analysis was performed using IDEAS software (EMD Millipore).

Endocytosis assays

Endocytosis assays were performed by measuring the loss of antibody-bound CIE cargo proteins from the cell surface over time. Jurkat T cells were pelleted and cooled in an ice bath for 10 min. Cold medium containing MHCI antibody and conjugated transferrin was added to the cells in the ice bath. Cells were incubated with the antibody and transferrin for 45 min to label all surface MHCI. Cells were rinsed three times in ice-cold PBS, and centrifuged at 180 ***g*** at 4°C for 10 min. Care was taken not to raise the temperature of the cells during the surface labeling and rinsing. Warm medium containing conjugated transferrin was added to the cells and they

were then incubated in a 37°C water bath for indicated times. Cells were removed from the water bath, returned to the ice bath, and centrifuged at 180 ***g*** at 4°C for 10 min. Cells were fixed in 4% formaldehyde, rinsed in PBS, and then in 10% FBS in PBS to reduce non-specific binding. Cells were incubated with a fluorescently tagged secondary antibody for 1 h without permeabilization and then examined by imaging flow cytometry. The mean surface intensity of surface MHCI was measured. Internalization was calculated as the percentage of surface MHCI lost from the surface as compared to the zero-time point.

Endocytosis in cells expressing dynamin constructs was measured directly by incubating the cells in a 37°C water bath with antibodies against MHCI and fluorescently conjugated transferrin. After 30 min, cells were pelleted and then rinsed for 8 s in 0.5% acetic acid and 0.5 M NaCl at pH 3.0 to remove surface-bound antibody and transferrin. pH was neutralized with NaOH in Hank's buffered saline solution and the cells were then fixed in 4% formaldehyde for 15 min. Cells were further processed for imaging flow cytometry.

Jurkat–Raji cell conjugate formation

Raji cells were incubated with 2 µg/ml of staphylococcal enterotoxin E (SEE; Toxin Technologies) for 30 min in a 37°C water bath in a 5 ml snap cap tube. Cells were rinsed once in serum-free medium and then re-suspended in 1 ml of serum free media. Raji cells were incubated at 37°C for 15 min in the presence of 0.5 µM Cell Tracker Blue CMAC Dye and fresh SEE. Raji cells were rinsed twice in warm complete medium. Cells were pelleted and re-suspended in 1 ml of complete medium. Raji cells were then incubated with Jurkat cells in 300 µl of complete medium in 15 ml snap cap tube at a ratio of one Jurkat cell to two Raji cells. Conjugates were incubated for the indicated times and plated on poly-L-lysine-coated coverslips for immunofluorescence or fixed in suspension and processed for imaging flow cytometry.

Spreading assays

Poly-L-lysine-coated coverslips were incubated with 10 µg/ml Biolegend mouse anti-CD3 (clone OKT3) in PBS overnight at 4°C. Coverslips were rinsed twice in PBS, and cells were plated at a concentration of 2×10^5 cells/ml in 200 µl of medium. Coverslips were placed in a 37°C water bath for 3 min and then fixed in 4% formaldehyde for 15 min. Coverslips were processed for immunofluorescence by blocking in 10% FBS in PBS for 20 min. To label the plasma membrane, coverslips were then incubated with Cell Mask™ Deep Red plasma membrane stain (1:750) in the presences of 0.02% saponin in 10% FBS in PBS for at least 1 h. Coverslips were then washed and mounted as described above. Coverslips were then imaged with the Zeiss LSM780 with a 63×1.4 NA Plan-Apochromat oil immersion objective lens with tiling. The area of cell spread was quantified for cells expressing GFP constructs only using Metamorph (Molecular Devices). Statistical analysis was performed with Graphpad Prism (Graphpad Software, Inc).

Acknowledgements

We thank Larry Samelson and Lakshmi Balagopalan (NCI) for advice and reagents for working with T cells. We also thank Lois Greene and members of the Donaldson laboratory for comments on the manuscript. Microscopes used in this study are part of the NHLBI Light Microscopy Facility, and imaging flow cytometry was conducted in the NHLBI Flow Cytometry Core.

Competing interests

The authors declare no competing or financial interests.

Author contributions

Conceptualization: D.L.J., J.W., J.M.W., J.G.D.; Methodology: D.L.J., J.W., J.G.D.; Formal analysis: D.L.J., J.W., J.M.W., J.G.D.; Investigation: D.L.J., J.W.; Data curation: D.L.J., J.W.; Writing - original draft: D.L.J., J.W., J.G.D.; Writing - review & editing: D.L.J., J.W., J.M.W., J.G.D.; Visualization: D.L.J., J.W.; Supervision: J.M.W., J.G.D.

Funding

This work was supported by the Intramural Research Program in the National Heart, Lung, and Blood Institute at the National Institutes of Health (NIH) (HL0006060) to JGD and by NIH grant RO1 DK084047 to J.M.W. Deposited in PMC for release after 12 months.

Supplementary information

Supplementary information available online at
http://jcs.biologists.org/lookup/doi/10.1242/jcs.200477.supplemental

References

Balagopalan, L., Barr, V. A. and Samelson, L. E. (2009). Endocytic events in TCR signaling: focus on adapters in microclusters. *Immunol. Rev.* **232**, 84-98.

Barral, D. C., Cavallari, M., McCormick, P. J., Garg, S., Magee, A. I., Bonifacino, J. S., De Libero, G. and Brenner, M. B. (2008). CD1a and MHC class I follow a similar endocytic recycling pathway. *Traffic* **9**, 1446-1457.

Blander, J. M. (2016). The comings and goings of MHC class I molecules herald a new dawn in cross-presentation. *Immunol. Rev.* **272**, 65-79.

Bouchet, J., del Rio-Iñiguez, I., Lasserre, R., Agüera-Gonzalez, S., Cuche, C., Danckaert, A., McCaffrey, M. W., Di Bartolo, V. and Alcover, A. (2016). Rac1-Rab11-FIP3 regulatory hub coordinates vesicle traffic with actin remodeling and T-cell activation. *EMBO J.* **35**, 1160-1174.

Brown, F. D., Rozelle, A. L., Yin, H. L., Balla, T. and Donaldson, J. G. (2001). Phosphatidylinositol 4,5-bisphosphate and Arf6-regulated membrane traffic. *J. Cell Biol.* **154**, 1007-1017.

Cai, E., Marchuk, K., Beemiller, P., Beppler, C., Rubashkin, M. G., Weaver, V. M., Gérard, A., Liu, T. L., Chen, B. C., Betzig, E. et al. (2017). Visualizing dynamic microvillar search and stabilization during ligand detection by T cells. *Science* **356**, eaal3118.

Cebrian, I., Croce, C., Guerrero, N. A., Blanchard, N. and Mayorga, L. S. (2016). Rab22a controls MHC-I intracellular trafficking and antigen cross-presentation by dendritic cells. *EMBO Rep.* **17**, 1753-1765.

Chaineau, M., Ioannou, M. S. and McPherson, P. S. (2013). Rab35: GEFs, GAPs and effectors. *Traffic* **14**, 1109-1117.

Cohen, L. A., Honda, A., Varnai, P., Brown, F. D., Balla, T. and Donaldson, J. G. (2007). Active Arf6 recruits ARNO/cytohesin GEFs to the PM by binding their PH domains. *Mol. Biol. Cell* **18**, 2244-2253.

Crotzer, V. L., Mabardy, A. S., Weiss, A. and Brodsky, F. M. (2004). T cell receptor engagement leads to phosphorylation of clathrin heavy chain during receptor internalization. *J. Exp. Med.* **199**, 981-991.

Das, V., Nal, B., Dujeancourt, A., Thoulouze, M.-I., Galli, T., Roux, P., Dautry-Varsat, A. and Alcover, A. (2004). Activation-induced polarized recycling targets T cell antigen receptors to the immunological synapse; involvement of SNARE complexes. *Immunity* **20**, 577-588.

Devés, R. and Boyd, C. A. R. (2000). Surface antigen CD98(4F2): not a single membrane protein, but a family of proteins with multiple functions. *J. Membr. Biol.* **173**, 165-177.

Dutta, D. and Donaldson, J. G. (2015). Sorting of clathrin-independent cargo proteins depends on Rab35 delivered by clathrin-mediated endocytosis. *Traffic* **16**, 994-1009.

Eyster, C. A., Higginson, J. D., Huebner, R., Porat-Shliom, N., Weigert, R., Wu, W. W., Shen, R.-F. and Donaldson, J. G. (2009). Discovery of new cargo proteins that enter cells through clathrin-independent endocytosis. *Traffic* **10**, 590-599.

Friedl, P. and Storim, J. (2004). Diversity in immune-cell interactions: states and functions of the immunological synapse. *Trends Cell Biol.* **14**, 557-567.

Grant, B. D. and Donaldson, J. G. (2009). Pathways and mechanisms of endocytic recycling. *Nat. Rev. Mol. Cell Biol.* **10**, 597-608.

Griffiths, G. M., Tsun, A. and Stinchcombe, J. C. (2010). The immunological synapse: a focal point for endocytosis and exocytosis. *J. Cell Biol.* **189**, 399-406.

Guedj, C., Abraham, N., Jullié, D. and Randriamampita, C. (2016). T cell adhesion triggers an early signaling pole distal to the immune synapse. *J. Cell Sci.* **129**, 2526-2537.

Honda, A., Al-Awar, O. S., Hay, J. C. and Donaldson, J. G. (2005). Targeting of Arf-1 to the early Golgi by membrin, an ER-Golgi SNARE. *J. Cell Biol.* **168**, 1039-1051.

Kauppi, M., Simonsen, A., Bremnes, B., Vieira, A., Callaghan, J., Stenmark, H. and Olkkonen, V. M. (2002). The small GTPase Rab22 interacts with EEA1 and controls endosomal membrane trafficking. *J. Cell Sci.* **115**, 899-911.

Kolanus, W., Nagel, W., Schiller, B., Zeitlmann, L., Godar, S., Stockinger, H. and Seed, B. (1996). Alpha L beta 2 integrin/LFA-1 binding to ICAM-1 induced by cytohesin-1, a cytoplasmic regulatory molecule. *Cell* **86**, 233-242.

Liu, H., Rhodes, M., Wiest, D. L. and Vignali, D. A. A. (2000). On the dynamics of TCR:CD3 complex cell surface expression and downmodulation. *Immunity* **13**, 665-675.

Magadan, J. G., Barbieri, M. A., Mesa, R., Stahl, P. D. and Mayorga, L. S. (2006). Rab22a regulates the sorting of transferrin to recycling endosomes. *Mol. Cell. Biol.* **26**, 2595-2614.

Maldonado-Báez, L. and Donaldson, J. G. (2013). Hook1, microtubules, and Rab22: mediators of selective sorting of clathrin-independent endocytic cargo proteins on endosomes. *Bioarchitecture* **3**, 141-146.

Maldonado-Báez, L., Cole, N. B., Krämer, H. and Donaldson, J. G. (2013a). Microtubule-dependent endosomal sorting of clathrin-independent cargo by Hook1. *J. Cell Biol.* **201**, 233-247.

Maldonado-Baez, L., Williamson, C. and Donaldson, J. G. (2013b). Clathrin-independent endocytosis: a cargo-centric view. *Exp. Cell Res.* **319**, 2759-2769.
Mayor, S., Parton, R. G. and Donaldson, J. G. (2014). Clathrin-independent pathways of endocytosis. *Cold Spring Harbor Perspect. Biol.* **6**, 93-112.
Miller, M. J., Safrina, O., Parker, I. and Cahalan, M. D. (2004). Imaging the single cell dynamics of CD4+ T cell activation by dendritic cells in lymph nodes. *J. Exp. Med.* **200**, 847-856.
Naj, X. and Linder, S. (2015). ER-coordinated activities of Rab22a and Rab5a drive phagosomal compaction and intracellular processing of borrelia burgdorferi by macrophages. *Cell Rep.* **12**, 1816-1830.
Naslavsky, N., Weigert, R. and Donaldson, J. G. (2003). Convergence of non-clathrin- and clathrin-derived endosomes involves Arf6 inactivation and changes in phosphoinositides. *Mol. Biol. Cell* **14**, 417-431.
Naslavsky, N., Weigert, R. and Donaldson, J. G. (2004). Characterization of a nonclathrin endocytic pathway: membrane cargo and lipid requirements. *Mol. Biol. Cell* **15**, 3542-3552.
Osborne, D. G., Piotrowski, J. T., Dick, C. J., Zhang, J. S. and Billadeau, D. D. (2015). SNX17 affects T cell activation by regulating TCR and integrin recycling. *J. Immunol.* **194**, 4555-4566.
Patino-Lopez, G., Dong, X., Ben-Aissa, K., Bernot, K. M., Itoh, T., Fukuda, M., Kruhlak, M. J., Samelson, L. E. and Shaw, S. (2008). Rab35 and its GAP EPI64C in T cells regulate receptor recycling and immunological synapse formation. *J. Biol. Chem.* **283**, 18323-18330.
Pelchen-Matthews, A., Parsons, I. J. and Marsh, M. (1993). Phorbol ester-induced downregulation of CD4 is a multistep process involving dissociation from p56lck, increased association with clathrin-coated pits, and altered endosomal sorting. *J. Exp. Med.* **178**, 1209-1222.
Pitcher, C., Honing, S., Fingerhut, A., Bowers, K. and Marsh, M. (1999). Cluster of differentiation antigen 4 (CD4) endocytosis and adaptor complex binding require activation of the CD4 endocytosis signal by serine phosphorylation. *Mol. Biol. Cell* **10**, 677-691.
Powelka, A. M., Sun, J., Li, J., Gao, M., Shaw, L. M., Sonnenberg, A. and Hsu, V. W. (2004). Stimulation-dependent recycling of integrin β1 regulated by ARF6 and Rab11. *Traffic* **5**, 20-36.
Radhakrishna, H. and Donaldson, J. G. (1997). ADP-ribosylation factor 6 regulates a novel plasma membrane recycling pathway. *J. Cell Biol.* **139**, 49-61.
Radhakrishna, H., Klausner, R. D. and Donaldson, J. G. (1996). Aluminum fluoride stimulates surface protrusions in cells overexpressing the ARF6 GTPase. *J. Cell Biol.* **134**, 935-947.
Ratcliffe, C. D. H., Sahgal, P., Parachoniak, C. A., Ivaska, J. and Park, M. (2016). Regulation of cell migration and beta1 integrin trafficking by the endosomal adaptor GGA3. *Traffic* **17**, 670-688.
Santy, L. C. and Casanova, J. E. (2001). Activation of ARF6 by ARNO stimulates epithelial cell migration through downstream activation of both Rac1 and phospholipase D. *J. Cell Biol.* **154**, 599-610.
Song, J., Khachikian, Z., Radhakrishna, H. and Donaldson, J. G. (1998). Localization of endogenous ARF6 to sites of cortical actin rearrangement and involvement of ARF6 in cell spreading. *J. Cell Sci.* **111**, 2257-2267.
Tzachanis, D., Appleman, L. J., Van Puijenbroek, A., Berezovskaya, A., Nadler, L. M. and Boussiotis, V. A. (2003). Differential localization and function of ADP-ribosylation factor-6 in anergic human T cells: a potential marker for their identification. *J. Immunol.* **171**, 1691-1696.
Walseng, E., Bakke, O. and Roche, P. A. (2008). Major histocompatibility complex class II-peptide complexes internalize using a clathrin- and dynamin-independent endocytosis pathway. *J. Biol. Chem.* **283**, 14717-14727.
Wang, L., Liang, Z. and Li, G. (2011). Rab22 controls NGF signaling and neurite outgrowth in PC12 cells. *Mol. Biol. Cell* **22**, 3853-3860.
Wang, T., Gilkes, D. M., Takano, N., Xiang, L., Luo, W., Bishop, C. J., Chaturvedi, P., Green, J. J. and Semenza, G. L. (2014). Hypoxia-inducible factors and RAB22A mediate formation of microvesicles that stimulate breast cancer invasion and metastasis. *Proc. Natl. Acad. Sci. USA* **111**, E3234-E3242.
Weigert, R., Yeung, A. C., Li, J. and Donaldson, J. G. (2004). Rab22a regulates the recycling of membrane proteins internalized independently of clathrin. *Mol. Biol. Cell* **15**, 3758-3770.
Zhu, J. and Paul, W. E. (2008). CD4 T cells: fates, functions, and faults. *Blood* **112**, 1557-1569.
Zhu, H., Liang, Z. and Li, G. (2009). Rabex-5 is a Rab22 effector and mediates a Rab22-Rab5 signaling cascade in endocytosis. *Mol. Biol. Cell* **20**, 4720-4729.
Zimmermann, P., Zhang, Z., Degeest, G., Mortier, E., Leenaerts, I., Coomans, C., Schulz, J., N'Kuli, F., Courtoy, P. J. and David, G. (2005). Syndecan recycling is controlled by syntenin-PIP2 interaction and Arf6. *Dev. Cell* **9**, 377-388.